Nanoscale live-cell imaging using hopping probe ion conductance microscopy

Pavel Novak[1,2,7], Chao Li[3,7], Andrew I Shevchuk[1], Ruben Stepanyan[4], Matthew Caldwell[5,6], Simon Hughes[5], Trevor G Smart[5], Julia Gorelik[2], Victor P Ostanin[3], Max J Lab[1], Guy W J Moss[5,6], Gregory I Frolenkov[4], David Klenerman[3] & Yuri E Korchev[1]

We describe hopping mode scanning ion conductance microscopy that allows noncontact imaging of the complex three-dimensional surfaces of live cells with resolution better than 20 nm. We tested the effectiveness of this technique by imaging networks of cultured rat hippocampal neurons and mechanosensory stereocilia of mouse cochlear hair cells. The technique allowed examination of nanoscale phenomena on the surface of live cells under physiological conditions.

There is a great interest in developing methods to image live cells at nanoscale resolution. Scanning probe microscopy (SPM) is one approach to this problem and both atomic force microscopy (AFM) and scanning electrochemical microscopy (SECM) have been used to image live cells[1,2]. However, deformation of the soft and responsive cell by the AFM cantilever, particularly when imaging eukaryotic cells, represents a substantial problem for AFM. SECM, in contrast, involves no physical contact with the sample, but true topographic imaging of the convoluted surface of living cells with nanoscale resolution has not been reported. Scanning ion conductance microscopy (SICM)[3] is another form of SPM, which allows imaging of the cell surface under physiological conditions without physical contact and with a resolution of 3–6 nm[4,5]. Until now, SICM has been restricted to imaging relatively flat surfaces, as all other SPM techniques. This is because when the probe encounters a vertical structure, it inevitably collides with the specimen (**Fig. 1a**). Here we report a mode of SICM that allows nanoscale imaging of even the most convoluted surface structures.

SICM is based on the phenomenon that the ion flow through a sharp fluid-filled nanopipette is partially occluded when the pipette approaches the surface of a cell[3]. In conventional SICM, a nanopipette is mounted on a three-dimensional piezoelectric translation stage and automatic feedback control moves the pipette up or down to keep the pipette current constant (the set point) while the sample is scanned in *x* and *y* directions. Thus, a pipette-sample separation, typically equal to the pipette's inner radius, is maintained during imaging. In hopping probe ion conductance microscopy (HPICM), we no longer use continuous feedback. Instead, at each imaging point, the pipette approaches the sample from a starting position that is above any of the surface features (**Fig. 1b**). The reference current is measured while the pipette is well away from the surface. The pipette then approaches until the current is reduced by a predefined amount, usually 0.25–1%. The position of *z*-dimension actuator when the current achieves this reduction is recorded as the height of the sample at this imaging point. Typically, even at a 1% reduction of the current, the pipette is still at a distance of about one inner pipette radius from the surface. The *z*-dimension actuator then withdraws the pipette away from the surface and the sample is moved laterally to the next imaging point. By continuously updating the reference current while the pipette is away from the surface, the method automatically adjusts for any slow drifts in the pipette current.

We illustrate the benefits of HPICM in **Figure 1c,d**; we first imaged fixed cultured hippocampal neurons in the hopping mode (**Fig. 1d**) and then in the raster scan mode (**Fig. 1c**). In contrast to HPICM, the raster scan SICM analysis identified distortions in the cell body and axon and dendrites, and there were several lines in the image where the automatic feedback could not maintain a constant probe-to-sample distance. At these lines, the fine processes that we visualized by HPICM imaging (**Fig. 1d**) were later destroyed during SICM imaging (**Fig. 1c**).

In contrast to conventional raster scanning, HPICM has the additional advantage that the order of imaging pixels is not predetermined. Therefore, we divided the entire image into equal-sized squares (**Fig. 1e**) and before imaging each square, we estimated the overall roughness (local height variation) of the sample by measuring the difference in heights at the corners of the square. If the sample within a square was rough, then we measured topography of this square at high resolution. If the sample was relatively flat, we imaged the square at lower resolution (**Fig. 1e**). These adaptive changes of resolution accelerated image acquisition without an apparent degradation of image quality. Additional acceleration can be achieved by adjusting the amplitude of probe withdrawal within each square so that it is just above the predetermined roughness of the sample within that square. The

[1]Division of Medicine, Imperial College London, London, UK. [2]National Heart and Lung Institute, Department of Cardiac Medicine, Imperial College London, London, UK. [3]Department of Chemistry, Cambridge University, Cambridge, UK. [4]Department of Physiology, University of Kentucky, Lexington, Kentucky, USA. [5]Department of Neuroscience, Physiology and Pharmacology, University College London, London, UK. [6]Centre for Mathematics and Physics in the Life Sciences and Experimental Biology, University College London, London, UK. [7]These authors contributed equally to this work. Correspondence should be addressed to Y.E.K. (y.korchev@imperial.ac.uk), D.K. (dk10012@cam.ac.uk) or G.I.F. (gregory.frolenkov@uky.edu).

RECEIVED 26 SEPTEMBER 2008; ACCEPTED 22 JANUARY 2009; PUBLISHED ONLINE 1 MARCH 2009; DOI:10.1038/NMETH.1306

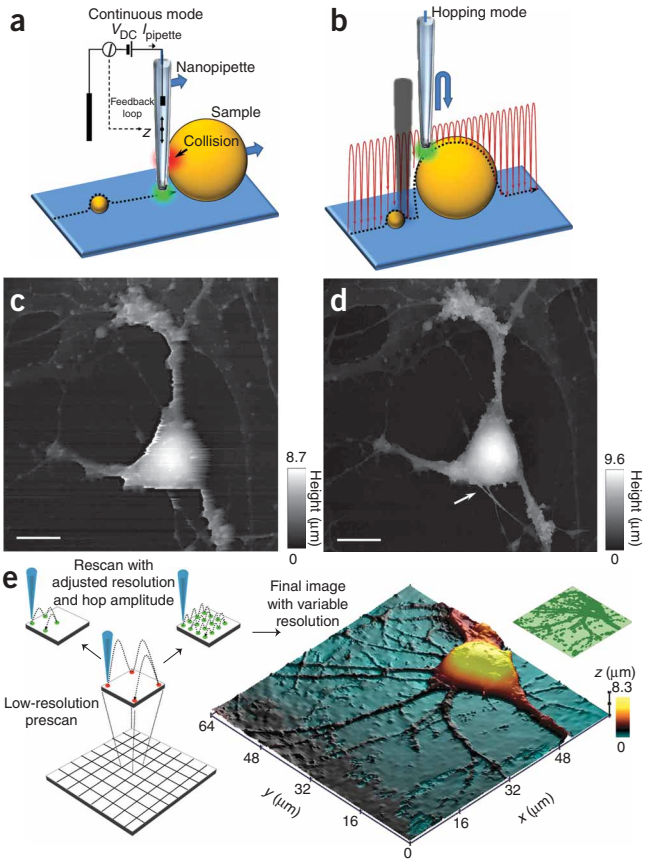

Figure 1 | Principles of adaptive HPICM. (**a**) Illustration of a scanning nanopipette probe operating in continuous scan mode colliding with a spherical object possessing a steep vertical slope. (**b**) Illustration of the hopping mode used in HPICM showing how the pipette is withdrawn to a position well above the sample before approaching the surface. (**c**,**d**) Topographical images of the same fixed hippocampal neuron obtained first with hopping mode (**d**) and then with continuous left-to-right raster scan mode (**c**), using the same nanopipette. Both images took 30 min to acquire. An arrow in **d** points to the fine processes that were damaged during raster scanning. Scale bars, 10 μm. (**e**) For adaptive HPCIM, the field of view was divided into equally sized squares (bottom left). Before imaging each square, the roughness of the sample in this square was estimated at the corners (middle left). Very rough squares were imaged at high resolution and smoother squares were imaged at low resolution (top left). A three-dimensional topographical rendered image of a hippocampal pyramidal neuron was acquired by the adaptive scanning algorithm (right). The inset (top right) shows the resolution that was used for imaging this neuron (high resolution in dark green, low resolution in light green).

smaller the amplitude of withdrawal, the faster is the imaging speed. We acquired an image of a hippocampal pyramidal neuron (**Fig. 1d**) by the adaptive scanning algorithm in 15 min, whereas imaging of the same sample without adaptive scanning would take 45 min. In contrast to raster scan techniques, adaptive HPICM also allows one to obtain a rapid low-resolution image of the sample to identify features of interest that will be subsequently imaged at high resolution.

To determine the robustness of our technique, we imaged the mechanosensitive stereocilia of the auditory hair cells in the cultured organ of Corti explants. Several attempts have been made previously to image stereocilia with AFM[6,7] or raster scan SICM (unpublished data; G.I.F., A.I.S., J.G. and Y.E.K.), but these studies had never resolved even a gross structure of the stereocilia bundle.

We used fixed specimens to compare images obtained with HPICM and using a scanning electron microscope (SEM) (**Fig. 2a–c** and **Supplementary Fig. 1** online). HPICM resolved stereocilia very well, including the shortest ones with a diameter of ~100 nm or less (**Fig. 2b**,**c** and **Supplementary Fig 1b**,**c**). We also visualized a kinocilium (true cilium), present in these young postnatal auditory hair cells (**Fig. 2c**). To explore the resolution limits of HPICM, we imaged fine extracellular filaments (links) that interconnect stereocilia and are crucial for their mechanosensory function. These links could be as small as ~8–10 nm in diameter[8]. In wild-type hair cells, most of the links were inaccessible to the HPICM probe because the probe approaches vertically to the bundle. Therefore, we used abnormally short but still mechanosensitive stereocilia of Shaker 2 mice[9] (**Fig. 2d–f**). Using our HPICM probe with an inner diameter of ~30 nm we resolved these links that appeared as features of 16 ± 5 nm (n = 37) in diameter (**Fig. 2f**). A resolution better than the inner diameter of the probe is not surprising because previously we had achieved a lateral resolution of 3–6 nm with a 12.5 nm diameter SICM probe[5]. HPICM uses the same sensor as SICM and, therefore, shares the same physical principles that determine lateral and vertical resolution (see **Supplementary Methods** online for discussion on the resolution limitations). The apparent diameter of the

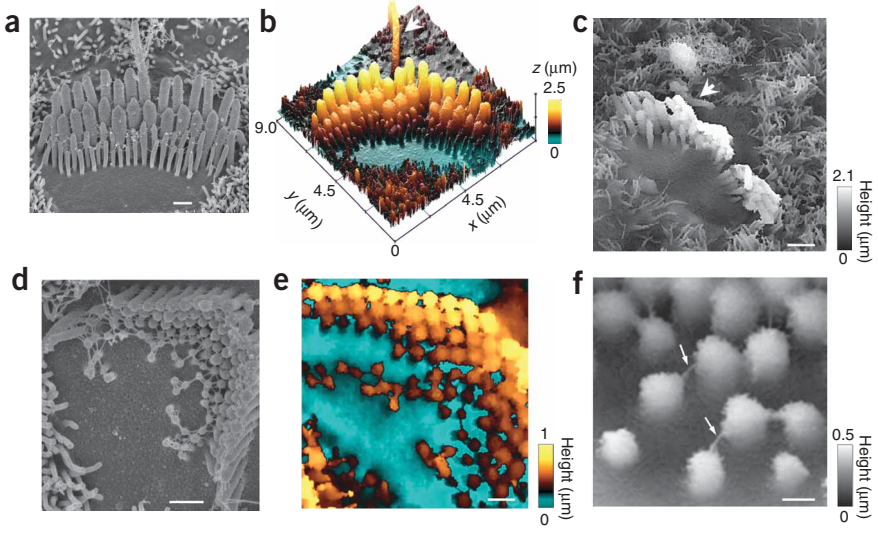

Figure 2 | Visualization of vertically protruding mechanosensitive stereocilia of auditory hair cells. (**a**–**c**) Stereocilia of wild-type inner hair cells. Arrow indicates a kinocilium (a true cilium). (**d**–**f**) Stereocilia of outer hair cells in young postnatal Shaker 2 mice with the extracellular filaments interconnecting stereocilia (arrows). All hair cells were approximately at the middle of the cochlea. Images of the cultured organs of Corti from the same mouse were obtained with SEM (**a**,**d**) and HPICM (**b**,**c**,**e**,**f**). Three-dimensional topographical rendered images are presented in colorscale (**b**,**e**) or grayscale (**c**,**f**). Scale bars, 500 nm (**a**,**d**,**e**), 1 μm (**c**) and 200 nm (**f**).

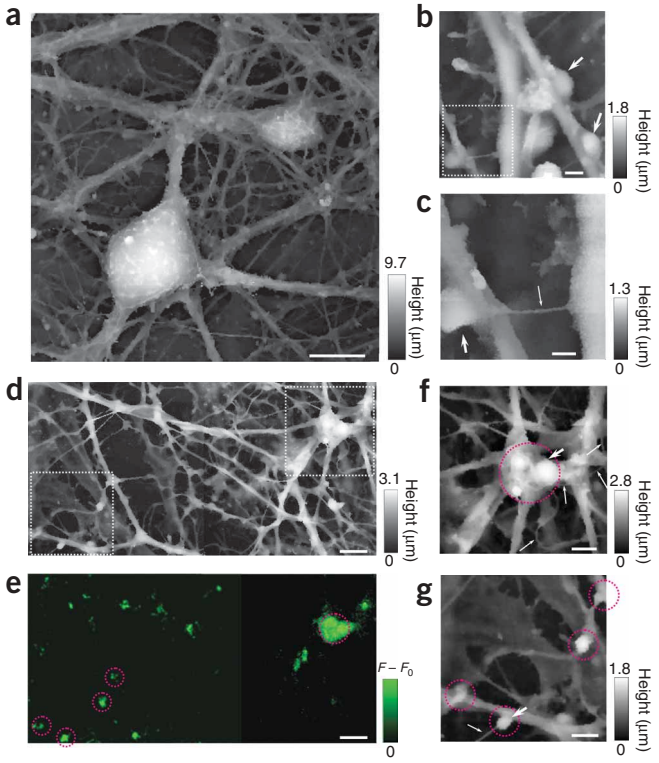

Figure 3 | HPICM images of live hippocampal neurons. (**a**) An image of a large area of a neural network. (**b**) An image of different area showing potential synaptic boutons (arrows). (**c**) A higher resolution image of the dotted region in **b** with another possible bouton (arrow). The process with a diameter of 50 nm (thin arrow) is likely to be an axon. (**d**,**e**) HPICM (**d**) and fluorescence (**e**) images of the same neuronal network area that has been stained with a live marker of synaptic activity, FM1-43. (**f**,**g**) High-resolution images of the dotted areas in **d** (top right, **f** and bottom left, **g**). Potential synaptic boutons are circled in red or marked with a large arrow. Fine processes, probably axons, are marked by thin arrows. Scale bars, 10 μm (**a**), 1 μm (**b**), 500 nm (**c**), 5 μm (**d**,**e**) and 2 μm (**f**,**g**). $F - F_0$ represents the fluorescence intensity above the background, F_0, in arbitrary units. The maximum value of $F - F_0$ was 50% of the dynamic range of the photomultiplier, and F_0 was 5%.

same stereocilia links on SEM images was 22 ± 5 nm ($n = 41$). After subtracting the platinum coat thickness (5 nm on both sides), we obtained an independent estimate of 12 ± 5 nm for the diameter of these links, in excellent agreement with HPICM.

Movements of live cells impose additional requirements for rapid imaging. To test whether adaptive HPICM is fast enough to visualize live complex cellular structures, we examined live hippocampal neurons (**Fig. 3a** and **Supplementary Fig. 2** online), which represent an unmet challenge for any scanning probe microscopy because of the complex three-dimensional shapes that are formed by axons and dendrites. HPICM revealed structures that resembled synaptic boutons as well as very fine (down to 50–60 nm in diameter) processes, tentatively identified as axons (**Fig. 3b**,**c**). We labelled this specimen with FM1-43, an activity-dependent marker of synaptic vesicles, and recorded the topography and the FM1-43 fluorescence. Whenever we observed a fluorescent signal, we could identify varicosities in our images (**Fig. 3d–g** and **Supplementary Fig. 3a–c** online). The size and shape of these varicosities was consistent with the geometry expected of synaptic boutons. It is thus clear that the speed of adaptive HPICM is sufficient to generate a 'snapshot' of axons, dendrites and boutons in these complex live networks in spite of relatively slow (on a time scale of tens of minutes) rearrangement and migration of the cells that occur in this preparation. Faster dynamics can be followed by imaging of a smaller area and/or decreasing the resolution. Additional developments should improve the temporal resolution of HPICM (**Supplementary Methods**).

HPICM is conceptually similar to 'force mapping' in AFM[10] or 'picking mode' in SECM[11]. However, force mapping AFM still detects a deflection of a cantilever, which implies a mechanical force applied to a cell. External force is not acceptable in most physiologically relevant experiments with soft and often mechanosensitive live eukaryotic cells. The picking mode SECM does not involve physical interaction between the probe and sample, but the relatively large insulation of SECM nanoelectrode[12] and its larger resistance, compared to SICM nanopipette of the same effective diameter, make topographic nanoscale imaging of convoluted cell surfaces with SECM a challenging and yet unresolved task.

The ability of HPICM to image complex biological samples at nanoscale resolution can be combined with fluorescent imaging[13] and/or other functional tests, such as local activation of individual receptors (ion channels)[14] or single-channel patch-clamp recordings[15] to enable structure-function studies at the surface of complex living cells with nanometer precision.

Note: Supplementary information is available on the Nature Methods website.

ACKNOWLEDGMENTS

This study was supported by the UK Biotechnology and Biological Sciences Research Council and Medical Research Council to Y.E.K. and (BB/D01817X/1) to G.W.J.M. and T.G.S., and by the US National Organization for Hearing Research Foundation, the Kentucky Science and Engineering Foundation (KSEF-148-502-07-215) and National Institute on Deafness and Other Communication Disorders, National Institutes of Health (DC008861 to G.I.F.).

AUTHOR CONTRIBUTIONS

P.N., C.L., A.I.S. and V.P.O. implemented experimental design into the hardware and the software; P.N., A.I.S., R.S., M.C. and S.H. performed the experiments; G.I.F., D.K., G.W.J.M., T.G.S., M.J.L., J.G. and Y.E.K. designed the study; P.N., G.I.F., D.K., G.W.J.M., T.G.S., M.J.L. and Y.E.K. wrote the paper.

COMPETING INTERESTS STATEMENT

The authors declare competing financial interests: details accompany the full-text HTML version of the paper at http://www.nature.com/naturemethods/.

Published online at http://www.nature.com/naturemethods/
Reprints and permissions information is available online at http://npg.nature.com/reprintsandpermissions/

1. Dufrene, Y.F. *Nat. Rev. Microbiol.* **6**, 674–680 (2008).
2. Sun, P. *et al. Proc. Natl. Acad. Sci. USA.* **105**, 443–448 (2008).
3. Hansma, P.K., Drake, B., Marti, O., Gould, S.A. & Prater, C.B. *Science* **243**, 641–643 (1989).
4. Korchev, Y.E., Bashford, C.L., Milovanovic, M., Vodyanoy, I. & Lab, M.J. *Biophys. J.* **73**, 653–658 (1997).
5. Shevchuk, A.I. *et al. Angew. Chem. Int. Ed. Engl.* **45**, 2212–2216 (2006).
6. Langer, M.G. *et al. Ultramicroscopy* **82**, 269–278 (2000).
7. Langer, M.G. *et al. Biophys. J.* **80**, 2608–2621 (2001).
8. Kachar, B., Parakkal, M., Kurc, M., Zhao, Y. & Gillespie, P.G. *Proc. Natl. Acad. Sci. USA.* **97**, 13336–13341 (2000).
9. Stepanyan, R., Belyantseva, I.A., Griffith, A.J., Friedman, T.B. & Frolenkov, G.I. *J. Physiol* **576**, 801–808 (2006).
10. van der Werf, K.O. *et al. Appl. Phys. Lett.* **65**, 1195–1197 (1994).
11. Borgwarth, K., Ebling, D.G. & Heinze, J. *Berichte der Bunsen-Gesellschaft Physical Chemistry Chemical Physics* **98**, 1317–1321 (1994).
12. Sun, P. & Mirkin, M.V. *Anal. Chem.* **78**, 6526–6534 (2006).
13. Gorelik, J. *et al. Proc. Natl. Acad. Sci. USA* **99**, 16018–16023 (2002).
14. Korchev, Y.E., Negulyaev, Y.A., Edwards, C.R., Vodyanoy, I. & Lab, M.J. *Nat. Cell Biol.* **2**, 616–619 (2000).
15. Gorelik, J. *et al. Biophys. J.* **83**, 3296–3303 (2002).